X-ray diffraction profiles from axial nanowire heterostructures

V. M. Kaganer, M. Wölz, O. Brandt, L. Geelhaar, and H. Riechert
Paul-Drude Institut für Festkörperelektronik, Hausvogteiplatz 5–7, DE-10117 Berlin, Germany
(Received 9 March 2011; revised manuscript received 3 May 2011; published 28 June 2011)

X-ray diffraction peaks from nanowires with quantum disks inserted to form axial heterostructures are studied theoretically and experimentally. The peak profiles are calculated taking into account partial coherence of the x-ray beam, the orientational distribution of nanowires, their length distribution, fluctuations of the layer thicknesses, and microstrain. We show on the example of $In_xGa_{1-x}N$/GaN superlattices that the common ω-2θ symmetric Bragg scans with a laboratory diffractometer provide the determination of superstructure periods, quantum well thicknesses, and In concentrations. The proposed method allows us to study the nanowire structures in the same manner as it is commonly done for planar heterostructures.

DOI: 10.1103/PhysRevB.83.245321 PACS number(s): 61.05.cp, 61.46.Km, 68.65.Cd

I. INTRODUCTION

The wide interest in semiconductor nanowires is driven by their potential as building blocks for future nanoelectronic and nanophotonic devices. Such applications typically require rather complex heterostructures to provide carrier confinement and/or wave-guiding of light.[1] The nanowire geometry allows to form heterostructures either in the radial direction, by making coaxial structures, or along the wire in the axial direction, as a stack of disks. The growth of axial heterostructures has been successfully realized in a number of systems, particularly in InAs/InP,[2,3] Si/Ge,[4,5] GaP/GaAs,[6] and AlN/GaN.[7,8]

The fabrication of nanowire-based electronic and photonic devices requires a high-level control of the growth of such heterostructures. However, the growth of nanostructures with the help of self-organization phenomena inevitably leads to fluctuations in their size and structure, as will be discussed in the next section. Hence, it is essential to obtain statistically relevant information on the nanowire heterostructures. Since a single nanowire does not represent the whole ensemble, transmission electron microscopy studies are even more laborious than in planar film studies. In contrast, x-ray measurements collect scattering intensities from a large number of nanowires and inherently perform this statistical average. Therefore, x-ray diffraction should play an important role in the structural determination of nanowire heterostructures. At the same time, the disorder in nanowire ensembles has a serious impact also on x-ray measurements.

X-ray diffraction has been used to study various aspects of nanowire structures. It was applied to obtain the epitaxial relationship between the nanowire and the substrate,[9–11] the nanowire diameters,[12,13] their in-plane orientation distribution (twist),[13,14] composition[15] and relaxation[8,16,17] of the parts with different composition, and to reveal different crystalline phases (wurtzite and zinc blende).[3,10,18,19] Both axial[3,8,15] and radial (core-shell)[16,17] heterostructures were investigated. The works cited above, with several exceptions,[9,11,13,14] employed synchrotron x-ray diffraction, particularly in grazing incidence geometry[3,8,10,17,18] and with microfocused x-ray beam.[19]

The aim of the present work is to develop a method of analysis for nanowire axial heterostructures similar to the routine x-ray diffraction methods for planar heterostructures. We restrict ourselves to the common ω-2θ symmetric Bragg diffraction scans of a laboratory x-ray diffraction experiment. We calculate the superlattice peaks taking into account the orientational distribution of nanowires, their distribution in lengths, the microstrains in the nanowires, and fluctuations of the layer thicknesses. The diffraction peaks are calculated in the kinematic approximation, taking into account the coherence limits of the laboratory experiment. As an experimental example, we study $In_xGa_{1-x}N$/GaN heterostructures in self-induced nanowires on Si(111) substrate. The comparison of the measured and calculated diffraction patterns allows us to determine the superlattice period, the quantum well thickness, and the In content in it. Thus the proposed method enables us to characterize the nanowire structures in the same manner as it is commonly done for planar heterostructures.

II. FLUCTUATIONS IN NANOWIRE HETEROSTRUCTURES

An ensemble of self-assembled nanowires, containing axial heterostructures, possesses different kinds of disorder. First of all, the growth rates of the individual nanowires depend on their diameters,[20–22] shadowing of the incoming atomic flux by neighboring nanowires,[23] and competition between neighboring nanowires for the precursor species.[24–26] Moreover, the nanowire nucleation may occur for quite a long time, so that the individual nanowires start to grow at different time moments.[27–32] As a result, the initial part of the nanowire (the base), on which the heterostructure is to be grown, strongly fluctuates in length. In terms of planar heterostructures, that could be treated as a huge buffer layer roughness. During the growth of the heterostructures in the nanowires, the same reasons result in large fluctuations in the thicknesses of individual layers.

For device applications, it is typically desirable that the nanowires grow in the direction normal to the interface. However, depending on the epitaxial relation to the substrate, the nanowires may exhibit a broad range of orientations. The range of the nanowire tilt is directly obtained from the widths of x-ray rocking curves, and for the self-induced GaN nanowires considered here, it typically amounts to several degrees of arc.[14] As a result, only a small fraction of nanowires is in diffraction position. Below we give an estimate of this fraction.

The nanowire tilt also gives rise to coalescence;[33] because of the spread in their orientations, the growing nanowires

may touch each other and then continue to grow as a single nanowire of a larger diameter with an orientation different from the ones of the initial two nanowires. The coalescence broadens the nanowire diameter distribution. The joints are strain concentrators since the change of orientations of the crystal lattices of the two nanowires requires the introduction of dislocations or disclinations.

It is well established that the crystalline structure in nanowires can differ from the bulk structure of the same material; nanowires often suffer from polytypism between wurtzite and zinc blende structures and twin defects as well as stacking faults are very common.[3,10,18,19,34] Our experimental example, the $In_xGa_{1-x}N$/GaN heterostructure, possesses wurtzite structure both in bulk and in nanowires. However, the calculations that we perform for symmetric Bragg reflections are applicable to any structure since the symmetric Bragg reflections are not sensitive to the difference between the structures. Both wurtzite and zinc blende structures can be treated as a sequence of identical atomic layers in the growth direction, the difference in relative lateral displacements of the layers is not relevant. Our study of symmetric Bragg reflections is insensitive to the nanowire twist, which amounts to several degrees of arc.[14] The lateral order and the distribution of nanowire diameters also do not enter into the analysis.

III. EXPERIMENT

Self-induced GaN nanowires were grown on Si(111) substrates by plasma-assisted molecular beam epitaxy. Samples 1 and 2 were grown as follows. GaN nanowires were nucleated at 770 °C with fluxes of 4 nm/min Ga and 20 nm/min N. After one hour of growth, the Ga flux was interrupted and the substrate temperature decreased to 585 °C for the growth of the active region. Both samples were grown to contain six pairs of a 4 nm thick $In_xGa_{1-x}N$ quantum well and a 15 nm thick GaN barrier. The nanowires of sample 1 were nucleated directly on the Si(111) substrate after nitridation for 5 min. In sample 2, an AlN buffer layer was grown before the nanowire nucleation, to provide better alignment of the nanowires.

Figures 1(a) and 1(b) present scanning electron microscopy images of sample 1, and Fig. 1(c) sketches the structure. A broad distribution of the nanowire lengths is evident from Fig. 1(a). The thicknesses of individual layers in the heterostructure also strongly vary, as it follows from the analysis below. The range of nanowire orientations has been measured by x-ray diffraction as the full width at half maximum (FWHM) of the GaN(0002) rocking curve and amounts to 3° for sample 1 and 0.84° for sample 2. Figure 1(c) schematically shows the nanowire arrangement and also their coalescence. The coalesced nanowires can be easily recognized in Fig. 1(b) by their larger diameters and their irregular cross sections.

X-ray measurements were done using a Panalytical X'Pert system with Ge(220) hybrid monochromator and Ge(220) analyzer crystal and with CuKα_1 radiation. Symmetric Bragg ω-2θ scans at the GaN(0002) reflection for the samples 1 and 2 are shown in Fig. 2 by thick gray lines. The thin black lines are the fits to the model developed below. The bottom line in Fig. 2 shows, for comparison, the calculated diffraction pattern for a uniform planar film with nominally the same heterostructure as in sample 2. The difference between the diffraction profiles from the nanowires and from a film is a result of the disorder in nanowires. The aim of the next sections is to take into consideration different types of disorder and finally obtain the calculated diffraction profiles for nanowires presented in Fig. 2.

IV. COHERENCE

The total x-ray intensity scattered by an ensemble of nanowires depends on the coherence of the x-ray beam. If different nanowires are illuminated incoherently, a sum of intensities from individual nanowires should be calculated. However, if they are illuminated coherently, a sum of amplitudes needs to be taken. Let us therefore estimate the coherence volume and then the number of nanowires illuminated coherently. The coherence volume in real space is inverse to the volume in reciprocal space representing the instrumental resolution. It is limited by the angular spread of the wave vectors, given by the angular acceptance of the monochromator and the analyzer, and the range of the wave vectors, determined by the wavelength range passed by the monochromator.

The transverse coherence length $l_t = \lambda/\Delta\theta$ is determined by the x-ray beam divergence $\Delta\theta$, where λ is the wavelength. In a laboratory x-ray diffraction setup, the transverse coherence lengths are strongly different in the scattering plane and in the direction normal to it. In the scattering plane, the x-ray beam is conditioned by the dynamical scattering from the monochromator and the analyzer crystals. The coherence length in the scattering plane $l_{t1} = \lambda/\Delta\theta_1$ is determined by the convolution of the Darwin widths of the monochromator and

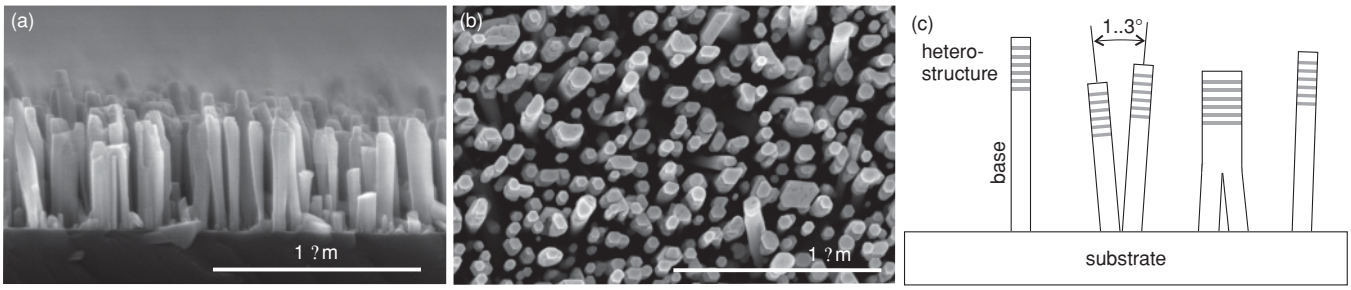

FIG. 1. Scanning electron microscopy (a) side and (b) top views of sample 1 and (c) schematics of the nanowire structure and arrangement.

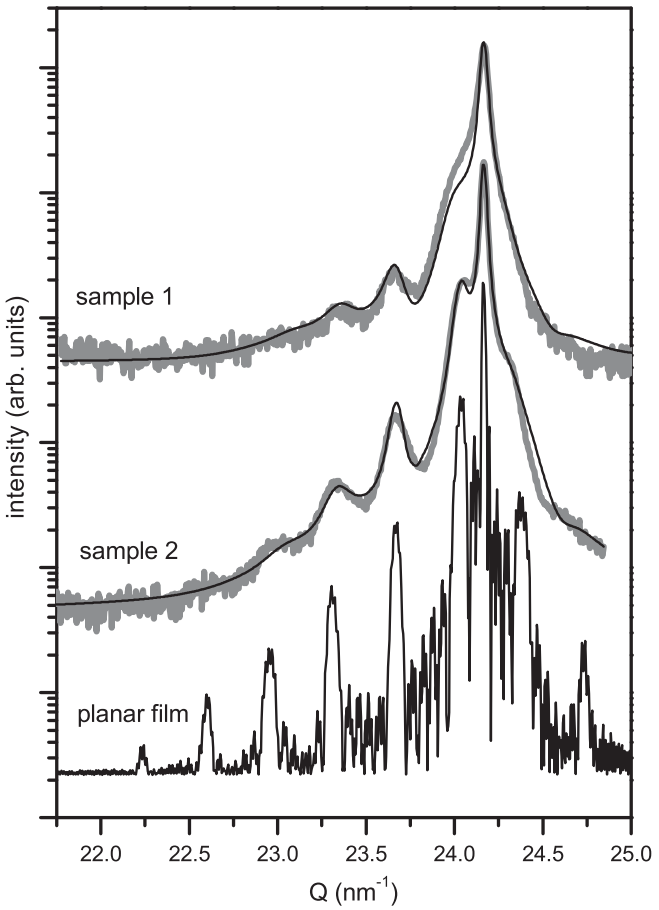

FIG. 2. X-ray diffraction profiles of samples 1 and 2: the experimental profiles (thick gray lines), the calculated profiles (thin black lines), and a calculated profile for an ideal planar heterostructure without fluctuations of the layer thicknesses (bottom line). The curves are shifted vertically for clarity.

the analyzer.[35] The measurement of the Si(111) reflection from a perfect crystal on our diffractometer gives $\Delta\theta_1 = 25''$, which results in $l_{t1} = 1.3\ \mu$m. In the direction normal to the scattering plane, the x-ray beam is not collimated and its divergence is much larger, $\Delta\theta_2 = 2^\circ$. The corresponding coherence length is very small, $l_{c2} = 4.4$ nm.

The longitudinal (temporal) coherence length $l_l = \lambda^2/\Delta\lambda$ is given by the spectral width $\Delta\lambda/\lambda$ of the radiation passing the monochromator. By measuring ω-2θ scans from a series of hhh reflections from a perfect Si(111) crystal, we have found the wavelength range $\Delta\lambda/\lambda \approx 2.4 \times 10^{-4}$, which gives $l_l = 0.64\ \mu$m. The longitudinal and tranverse coherence lengths are comparable just because the diffractometer is designed to provide close resolutions in different directions in the scattering plane.

Thus we consider for further estimates the coherence volume in the laboratory experiment as a disk lying in the scattering plane of a diameter approximately 1 μm and a thickness in the direction normal to the scattering plane of just a few nanometers. The scale bar in Fig. 1(b) can itself be considered as a sample of coherently illuminated area. Taking the mean distance between nanowires of 100 nm, we conclude that up to 10 nanowires are illuminated coherently. It is worth to mention that Fig. 1(b) represents the case of fairly large nanowire density and just one nanowire can be illuminated coherently for other material systems. In a synchrotron x-ray diffraction experiment, the coherence is provided by the angular width of the x-ray source, located at a large distance from the experiment, and amounts to several microns in any direction on the sample surface. All nanowires contained in the sample area of several μm^2, which are several hundreds of nanowires, will be illuminated coherently. In a synchrotron x-ray scattering study of SiGe Stranski-Krastanov islands,[36] an interference has been observed between the waves scattered by different islands within this area.

Let us estimate the fraction of nanowires contributing to the diffraction signal. To do that, we consider a nanowire as a cylinder, inclined by an angle ϕ to the surface normal, with the cylinder length large compared to the diameter. We calculate the scattered intensity that depends on ϕ and estimate the range of ϕ that contribute to diffraction. In the ω-2θ scan of a symmetric Bragg reflection, the x-ray momentum transfer Q is along the substrate surface normal. For a nanowire inclined by an angle ϕ to this direction, the components of the momentum transfer along and perpendicular to the nanowire are $Q_\parallel = Q\cos\phi$ and $Q_\perp = Q\sin\phi$, respectively.

We perform here the calculation of the nanowire structure factor in some detail, instead of writing down the well-known result, see Eq. (5), since we make use of the intermediate steps in the next sections. The x-ray scattering amplitude $A(Q)$ can be written as a sum over unit cells of the nanowire,

$$A(Q) = f \sum_{m,n,k} \exp[i(\mathbf{Q}_\perp \cdot \boldsymbol{\rho}_{mn} + Q_\parallel kd)], \qquad (1)$$

where f is the structure amplitude of the unit cell and $\boldsymbol{\rho}_{mn} = (ma, na)$ is a two-dimensional vector in the lateral plane of the nanowire, a is the lattice spacing in this plane. The lattice spacing along the nanowire d corresponds to the actual reflection Q, so that the difference $q = Q_\parallel - 2\pi/d$ is small. Since $Q_\perp$ is small because of a small range of nanowire orientations, the sum (1) can be written as a product of integrals over the nanowire volume,

$$A(Q) = f \int_0^t \exp(iqz)\, dz \int_{|\boldsymbol{\rho}|<D/2} \exp\left[i\,(\mathbf{Q}_\perp \cdot \boldsymbol{\rho})\right]\, d\boldsymbol{\rho}, \quad (2)$$

where t is the nanowire length and D is its diameter. Calculating the integrals, we represent the scattering amplitude as a product of the longitudinal

$$A_\parallel(q) = f\frac{\exp(iqt) - 1}{iq} \qquad (3)$$

and the transverse

$$A_\perp(q_\perp) = J_1(Q_\perp D/2)/Q_\perp \qquad (4)$$

components, where $J_1(x)$ is the first order Bessel function. The unit cell structure amplitude f is arbitrarily ascribed to the longitudinal component to be consistent with the calculations for multilayer structures in Sec. VI where the layers in heterostructure have different structure amplitudes

f_n. The structure factor $S(Q) = |A(Q)|^2$ is also a product of the longitudinal and the transverse factors:

$$S_{\parallel}(q) = |f|^2 \left[\frac{\sin(qt/2)}{q}\right]^2 \text{ and } S_{\perp}(Q_{\perp}) = \left[\frac{J_1(Q_{\perp}D/2)}{Q_{\perp}}\right]^2. \quad (5)$$

The function $[J_1(x)/x]^2$ has a maximum at $x = 0$ and decreases by a factor of two at $x \approx 1.62$. To estimate the range of transverse momenta that contribute to the structure factor, we take $\pi/2$ instead of this latter value and obtain $Q_{\perp}D \leqslant \pi$. Since the angle ϕ is small, this condition can be rewritten as $|\phi| \leqslant \pi/(QD)$. Substituting $Q \approx 2\pi/d$, we find that the range of the nanowire orientations contributing to diffraction is limited by $|\phi| \leqslant \phi_0 = d/2D$. Taking the lattice spacing $d \simeq 0.26$ nm for the GaN(0002) reflection and a typical nanowire diameter $D \simeq 70$ nm, we find $\phi_0 = 0.1^\circ$. The range of the nanowire orientations contributing to diffraction $2\phi_0 = 0.2^\circ$ is to be compared with the total angular range of nanowire orientations Ω given by the width of the x-ray rocking curve. Since the solid angles are compared, the fraction of nanowires contributing to diffraction is $(2\phi_0/\Omega)^2$. For sample 1 with $\Omega = 3^\circ$, we find that one nanowire out of 200 contributes to the diffraction signal. Hence, only one nanowire per coherence volume may happen to be in diffraction conditions. For sample 2 with $\Omega = 0.8^\circ$, one nanowire out of 16 contributes to diffraction. As a result, a coherence volume contains one nanowire in diffraction conditions. Thus, the x-ray scattering intensity from our samples can be calculated as a sum of the scattering intensities from single nanowires. Better alignment of nanowires due to improvements in growth and better coherence of the x-ray beam in synchrotron experiments will provide more nanowires in the coherence volume. Below in Sec. VIII, we analyze the interference between waves scattered by several coherently illuminated nanowires and show that it results in an extinction of the diffraction signal.

The longitudinal momentum transfer $Q_{\parallel}$ for different nanowire orientations varies as $Q_{\parallel} = Q\cos\phi \simeq Q(1 - \phi^2/2)$. The actual range of orientations, $|\phi| \leqslant \phi_0$, gives rise to the variation of the product $Q_{\parallel}t/2$ by less than dt/D^2. With the lattice spacing d, the diameter D given above, and a nanowire length $t = 300$ nm the variation of $Q_{\parallel}t/2$ is less than 0.02. Hence, in the calculations below, we can neglect the difference between Q and $Q_{\parallel}$ in the definition of the reduced momentum transfer, $q = Q - 2\pi/d$.

V. MICROSTRAIN IN NANOWIRES

The peaks from the GaN base of the nanowires (the main peaks in Fig. 2) occur notably broader than the ones calculated by Eq. (5). Figure 3(a) compares the measured GaN base peaks from sample 2 with the calculation based on Eq. (5) with large fluctuations in the base length and the experimental resolution taken into account. To reveal the source of the peak broadening, we have measured three subsequent symmetric Bragg reflections. The peak width increases proportionally to the reflection order. This is illustrated by Fig. 3(b) where the momentum transfer q is scaled by the reflection order: for a reflection $000n$ with $n = 2,4,6$, the abscissa is q/n. The peaks coincide after such a scaling. This is a clear indication of strain

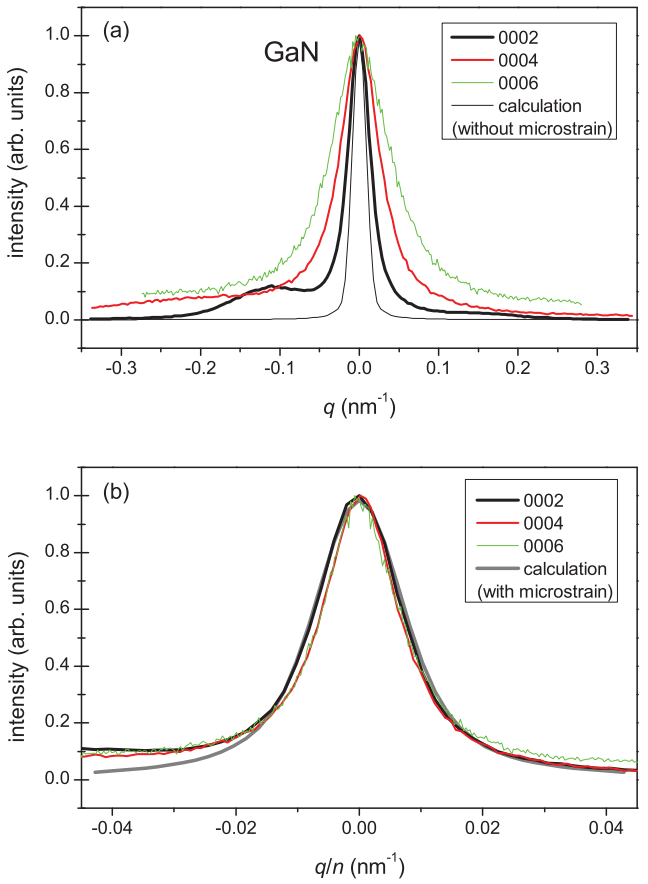

FIG. 3. (Color online) (a) Diffraction peaks of the three subsequent symmetric Bragg reflections from the GaN base layer of sample 2 and (b) the same peaks scaled by the reflection order.

fluctuations in nanowires as a source of the peak broadening, as it is discussed in detail below.

The diffraction peak broadening due to nonuniform fluctuating strain (microstrains) is well established in powder diffraction.[37,38] It is commonly assumed that the microstrains are caused by crystal lattice defects uniformly distributed in the powder grains and, hence, the mean-squared strains do not depend on the spatial position. The result is a Gaussian peak shape. However, the peaks in Fig. 3 are not Gaussian. Single nanowires are free from bulk defects but the nanowire coalescence gives rise to defects at the coalescence places.[33] The microstrain in a nanowire can also be caused by defects at the nanowire-substrate interface or in the parts of nanowires close to the interface.[32] In any case, the mean-squared microstrains are nonuniform. The aim of the present section is to extend the diffraction peak broadening due to microstrains[37,38] to the case of nonuniform microstrains and estimate the microstrain distribution based on the diffraction peaks in Fig. 3.

The crystal lattice defects may cause displacements of the atomic planes in the whole nanowire. These displacements can be taken into account by adding a random displacement u_k to the position of the kth atomic plane in Eq. (1). Each term in the sum (1) acquires an additional factor $\exp(i\,Qu_k)$. Hereafter we replace $Q_{\parallel}$ by Q, since the estimates in Sec. IV have shown

that the difference can be neglected. Proceeding from the sum (1) to the integral (2), we have now

$$A_{\parallel}(Q) = f \int_0^t \exp[iqz + iQu(z)]\, dz, \tag{6}$$

where $u(z)$ is the random displacement. It is worth to point out again that, to proceed to the continuous representation, Eq. (6), one has to introduce the small deviation $q = Q - 2\pi/d$ of the momentum transfer from the reciprocal lattice point. However, the displacement $u(z)$ remains to be multiplied with the momentum transfer Q (which can be replaced by $2\pi/d$ here).

The structure factor $S_{\parallel}(Q)$ is obtained by averaging $\left|A_{\parallel}(Q)\right|^2$ over the distribution of random displacements,

$$S_{\parallel}(Q) = |f|^2 \int\int_0^t \exp\left[iq(z_1 - z_2)\right] G(z_1, z_2)\, dz_1 dz_2, \tag{7}$$

where the correlation function is

$$G(z_1, z_2) = \langle \exp\left\{iQ\left[u(z_1) - u(z_2)\right]\right\}\rangle . \tag{8}$$

In the common approach,[37,38] the displacements $u(z)$ are considered as Gaussian random variables and the term in the angular brackets in Eq. (8) becomes

$$G(z_1, z_2) = \exp\left\{-\tfrac{1}{2} Q^2 \left\langle [u(z_1) - u(z_2)]^2 \right\rangle\right\} . \tag{9}$$

For closely spaced points z_1 and z_2, one expands

$$u(z_1) - u(z_2) \approx \epsilon(z_1 - z_2), \tag{10}$$

where ϵ is the random strain, and arrives at

$$G(z_1, z_2) = \exp\left\{-\tfrac{1}{2} Q^2 \langle \epsilon^2 \rangle (z_1 - z_2)^2\right\} . \tag{11}$$

Equation (11) shows that the contribution to the correlation function from large separations $z_1 - z_2$ is exponentially small, and the expansion (10) has to be performed in the actual range $|z_1 - z_2| \leqslant (Q^2 \langle \epsilon^2 \rangle)^{-1/2}$, which decreases with the increasing microstrain. It remains to integrate in Eq. (7) the Gaussian function (11) of the argument $\zeta = z_1 - z_2$ and arrive at the Gaussian diffraction peak shape $\propto \exp[-q^2/(2\langle \epsilon^2 \rangle Q^2)]$. Note that the peak width is proportional to the reflection order, $\Delta q \propto Q$, which is the fingerprint of the microstrain related peak broadening and justifies the choice of coordinates in Fig. 3(b).

The extensions[39,40] of this classical analysis consider the mean-squared strain not as a constant but a function of the separation $z_1 - z_2$. Particularly, an assumption $\langle \epsilon^2 \rangle \propto 1/(z_1 - z_2)$ gives rise to a Lorentzian peak shape but the order of reflection dependence becomes $\Delta q \propto Q^2$. To our knowledge, the spatial nonuniformity of the mean-squared strain was not considered. For nanowires, it is natural to assume that the mean-squared strains depend not on a small separation $\zeta = z_1 - z_2$ between the points where the correlation function $G(z_1, z_2)$ is calculated but on the absolute position $z = (z_1 + z_2)/2$ of these points. We therefore consider nonuniform mean-squared strains and denote

$$\varepsilon(z) = \langle \epsilon^2 \rangle^{1/2}. \tag{12}$$

Substituting Eq. (11) into Eq. (7), one can perform one integration analytically and arrive at

$$S_{\parallel}(Q) = \int_0^t \frac{dz}{\varepsilon(z)} \exp\left\{-\frac{1}{2}\left[\frac{q}{\varepsilon(z) Q}\right]^2\right\} . \tag{13}$$

The diffraction peak profile described by Eq. (13) preserves the linear scaling of the peak width with the reflection order, $\Delta q \propto Q$, for any function $\varepsilon(z)$.

Equation (13) contains a sum of intensities from sublayers with different rms microstrains $\varepsilon(z)$ and does not depend on positions and sequence of these sublayers. Having a function $\varepsilon(z)$ that describes an experimental diffraction profile, one cannot conclude which part of the nanowire is more strained on average, the top or the bottom. The function $\varepsilon(z)$ only represents the relative fractions of the nanowire parts with small and large microstrain.

The GaN base peak in Fig. 3 can be studied in a rather limited range of wave vectors, because of the heterostructure on top of it (cf. Fig. 2). We find that it can be adequately described by assuming that the mean-squared strains decay as z^{-1} with the distance, $\varepsilon(z) = \varepsilon_0 t/z$. The constant ε_0 describes the minimum strain fluctuations in the nanowire. An advantage of this functional form is the possibility to take the integral (13) analytically:

$$S_{\parallel}(Q) = \frac{|f|^2}{q^2}\left[1 - \exp\left(-\frac{q^2}{2\varepsilon_0^2 Q^2}\right)\right] . \tag{14}$$

The thick gray line in Fig. 3(b) shows the peak profile calculated by Eq. (14). This calculation provides the minimum microstrain of $\varepsilon_0 = 4 \times 10^{-4}$. A Williamson-Hall analysis of the peak widths in successive orders would give a close value for the rms strain since the half-width of the peak is determined by the less-strained parts of the nanowire. The more strained parts contribute to the tails of the peak profile. In other words, the Williamson-Hall analysis provides the microstrain fluctuations in the most ordered parts of the nanowires rather than an average over the whole nanowires.

The joints at the nanowire coalescence places are the sources of microstrain.[33] The joints in different nanowires occur on random heights, and Eq. (13) averages over their positions. The heterostructure also causes strain that decays with the distance from the heterostructure. Since the heterostructures in different nanowires are on different heights, Eq. (13) implies a corresponding average. The decay of the strain from both sources is expected to be exponential on distances much larger than the nanowire diameter but the main contribution to the integral (13) is from distances comparable with the diameter. The z^{-1} dependence just mimics a decay of the microstrain with distance from the joint or from the heterostructure. We do not have fundamental reasons for this functional form but the z^{-1} dependence is chosen to simplify numerical calculations by performing the analytical integration (14). Since the present work is primarily devoted to study heterostructures, the use of Eq. (14) provides a good enough agreement with the experimental curves. We do not consider an effect of microstrain on the diffraction peaks from the heterostructre since they are notably broader than the GaN base peak, cf. Fig. 2. The main source of their broadening is the fluctuation of the layer thicknesses described in the

next section. The presence of heterostructure severly limits the angular range of the x-ray profile where the microstrain effects can be measured. A more detailed analysis of microstrain performed on pure GaN nanowires that do not contain extra layers will be presented elsewhere.

VI. DIFFRACTION PEAKS FROM NANOWIRES WITH HETEROSTRUCTURES

The aim of this section is to calculate the diffraction profile from an ensemble of nanowires with nominally the same multilayer in each nanowire. The x-ray scattering of such nanowires differs from that of planar multilayers due to large fluctuations of the layer thicknesses. A large variance in nanowire heights is evident from Fig. 1(a), and the analysis below reveals large fluctuations of the layer thicknesses in the heterostructure. Our aim is to calculate the x-ray scattering intensity averaged over these fluctuations.

We assume in this section that only one nanowire is illuminated coherently, so that the intensity scattered by a single nanowire is to be averaged over thickness fluctuations. The generalization to the case of several coherently illuminated nanowires will be done in Sec. VIII. We use the results of Sec. IV that concern the transverse component of the structure factor and consider here only the longitudinal component. To simplify notation, we omit the subscript $\parallel$ in the scattering amplitude $A_\parallel(Q)$ and the structure factor $S_\parallel(Q)$.

Let us calculate the scattering amplitude and then the structure factor from a single nanowire. The nanowire containing a heterostructure is considered as a sequence of N layers, $n = 1, \ldots, N$, each layer consisting of M_n monolayers with the lattice spacing d_n and the structure amplitude of the unit cell f_n. We consider only symmetric Bragg reflections and d_n are the vertical spacings of fully strained epitaxial layers with different lattice parameters.

In the kinematic approximation, the contribution of the nth layer to the x-ray scattering amplitude is

$$A_n(Q) = f_n e^{iQ(M_1 d_1 + \cdots + M_{n-1} d_{n-1})} \sum_{k=1}^{M_n} e^{iQ d_n k}, \tag{15}$$

which generalizes the longitudinal factor in Eq. (1). The first exponential factor determines the height position of the bottom of the nth layer, while the sum takes into account the phase factors of each subsequent monolayer in it. To proceed to the continuous description as in Eqs. (2) and (3), let us define the layer thicknesses $t_n = d_n M_n$ and the wave vector deviations from the Bragg positions of the corresponding layers, $q_n = Q - 2\pi/d_n$. Since the deviations are small, one can proceed from the sum (15) to the integral

$$\begin{aligned} A_n(Q) &= f_n e^{i(q_1 t_1 + \cdots + q_{n-1} t_{n-1})} \int_0^{t_n} e^{iq_n z}\, dz \\ &= \frac{f_n}{iq_n}(e^{i\varphi_{1,n}} - e^{i\varphi_{1,n-1}}), \end{aligned} \tag{16}$$

where it is denoted

$$\varphi_{m,n} = \sum_{k=m}^{n} q_k t_k. \tag{17}$$

The total scattering amplitude is

$$A(Q) = \sum_{n=1}^{N} A_n(Q). \tag{18}$$

The structure factor for a single nanowire can be represented as

$$|A|^2 = \sum_{n=1}^{N} |A_n|^2 + \sum_{\substack{m,n=1 \\ m<n}}^{N} 2\mathrm{Re} A_m^* A_n. \tag{19}$$

Equation (16) gives

$$|A_n|^2 = \frac{|f_n|^2}{q_n^2}(2 - e^{iq_n t_n} - e^{-iq_n t_n}) \tag{20}$$

and, for $m < n$,

$$A_m^* A_n = \frac{f_m^* f_n}{q_m q_n}(e^{i\varphi_{m+1,n}} + e^{i\varphi_{m,n-1}} - e^{i\varphi_{m,n}} - e^{i\varphi_{m+1,n-1}}). \tag{21}$$

We keep the expression (20) in an exponential form rather than to simplify it as in Eq. (5), since Eq. (20) allows a simple average over the thickness fluctuations. The layer thicknesses t_n are considered as independent Gaussian random variables with the mean value $\bar{t}_n = \langle t_n \rangle$ and the dispersion $\sigma_n^2 = \langle (t_n - \bar{t}_n)^2 \rangle$. The Gaussian average for a single exponential term is $\langle \exp(iq_n t_n) \rangle = \exp(iq_n \bar{t}_n - q_n^2 \sigma_n^2/2)$. Since thickness fluctuations in different layers are statistically independent, the products are averaged as $\langle \exp(iq_m t_m + iq_n t_n) \rangle = \langle \exp(iq_m t_m) \rangle \langle \exp(iq_n t_n) \rangle$ for $m \neq n$. The average of Eqs. (20) and (21) is straightforward and we have finally

$$\begin{aligned} \langle |A|^2 \rangle &= \sum_{n=1}^{N} \langle |A_n|^2 \rangle + \sum_{\substack{m,n=1 \\ m<n}}^{N} 2\mathrm{Re} \langle A_m^* A_n \rangle, \\ \langle |A_n|^2 \rangle &= \frac{2\,|f_n|^2}{q_n^2}[1 - e^{-q_n^2 \sigma_n^2/2} \cos q_n \bar{t}_n], \\ \langle A_m^* A_n \rangle &= \frac{f_m^* f_n}{q_m q_n}(e^{\Phi_{m+1,n}} + e^{\Phi_{m,n-1}} - e^{\Phi_{m,n}} - e^{\Phi_{m+1,n-1}}), \end{aligned} \tag{22}$$

where it is denoted

$$\Phi_{m,n} = \sum_{k=m}^{n} \left(iq_k \bar{t}_k - q_k^2 \sigma_k^2 / 2 \right). \tag{23}$$

Equations (22) were used to calculate the diffraction patterns in Fig. 2. The parameters used in the calculations and further discussion are given in the next section.

VII. CALCULATION OF THE DIFFRACTION PEAKS

We return to the experimental x-ray diffraction profiles in Fig. 2 and describe the calculated curves in detail. The contribution of the bottom GaN layer (the base) is calculated by Eq. (14), which takes the microstrain into account. All further layers of the heterostructure are calculated using equations (22), where the thickness fluctuations are taken into account but the microstrain is ignored. This is justified by a comparison of the widths of the main peak and the satellites in Fig. 2. The satellites are notably broader, so that, if the same microstrains as in the base are included in the calculation, they cause only a small additional effect. The microstrain effect on the base peak

follows from the comparison of the successive reflection orders in Fig. 3. The intensity of the satellite reflections is too low to study the microstrains in the heterostructure by measuring the higher order reflections. Since, on average, the microstrains in the heterostructure can hardly be larger than in the base and since the satellite peaks are notably broader, the account of microstrain only in the base is a reasonable approximation.

The heterostructure is considered as a sequence of six identical double layers. The period, thickness of the well, and its vertical lattice spacing are obtained from the fits. The layer thickness fluctuations σ_n are assumed to be the same for all layers and are also obtained from the fits. The fits presented in Fig. 2 reveal slightly different superstructure periods for samples 1 and 2: 19 and 17.5 nm, respectively. The thickness of the $In_xGa_{1-x}N$ well is the same, 3.8 nm, and the difference in periods is due to the difference in the GaN spacer layers. The relative differences of the lattice spacings in the vertical direction $\Delta d/d$ between the well and the spacer layers are 0.037 and 0.027, respectively. Assuming that the supestructure is elastically relaxed both laterally and vertically, these values correspond to an In content of $x = 24$ and 18% in the wells of samples 1 and 2, respectively. The mean-squared thickness fluctuations of each layer in the heterostructure are found to be $\sigma = 2.4$ and 2.0 nm for samples 1 and 2, respectively.

The minimum microstrain of $\varepsilon_0 = 4 \times 10^{-4}$ for sample 2 has been already discussed in Sec. V above. For sample 1, we obtain the slightly larger value of 5×10^{-4}. The good agreement between measured and calculated curves in Fig. 2 demonstrates that despite the smoothing of details of the x-ray diffraction profiles by disorder, the standard laboratory symmetric Bragg ω-2θ scans provide detailed information on the nanowire structure.

The obtained information paves the way for an efficient development of functional nanowire heterostructures such as Bragg reflectors or active regions for light-emitting diodes. In polar quantum wells formed by c-plane $In_xGa_{1-x}N$, the thickness has a large effect on the light emission. Reliable structural information is required to distinguish the effects of quantum well thickness and composition on the light emission from other nanowire properties such as surface Fermi level pinning and size effects on wave propagation. Our analysis makes these data available and also points at the challenge of reducing the observed thickness fluctuations.

VIII. EXTINCTION

The coherence volume and the fraction of nanowires that contribute to diffraction were estimated in Sec. IV. It follows that, in the samples that we have investigated experimentally, about 10 nanowires are illuminated coherently in the laboratory x-ray diffraction experiment but just one of them contributes to diffraction. Then, the diffracted intensity is a sum of intensities from individual nanowires. The average of the intensity over the ensemble of nanowires is performed in Sec. VI. If the coherence volume is increased, particularly in a synchrotron-diffraction experiment, or the alignment of nanowires is improved, several nanowires within each coherence volume will contribute to diffraction. Hence, their scattering amplitudes, rather than intensities, have to be summed up. The total intensity from these coherently scattered nanowires has to be averaged further over a large number of coherence volumes illuminating the ensemble of nanowires.

The waves scattered by several coherently illuminated nanowires interfere and, on average over the nanowire ensemble, weaken the scattered intensity. The effects of extinction are well known in diffraction from polycrystals and subdivided, from the very first works on the topic,[41] to the primary and the secondary extinction. The primary extinction arises due to dynamical diffraction effects in scattering from large single grains, while the secondary extinction is due to shadowing of the grains by other grains of the same orientation. The interference of the waves scattered by different nanowires that we study here differs from these two classical extinction phenomena but also represents a kind of extinction. Similar effects are observed in the scattering from textured nanocrystalline materials.[42,43] The extinction described in this section has rather little effect for the samples that we have investigated experimentally but becomes essential with better alignment of nanowires or in synchrotron experiments. Our further analysis is devoted to the evaluation of the interference extinction.

Let N_c be the number of nanowires that coherently contribute to diffraction. Then, the scattering amplitude $A_{\rm tot}(Q)$ from a single coherence volume is the sum of scattering amplitudes of the nanowires,

$$A_{\rm tot} = \sum_{i=1}^{N_c} A^{(i)}. \tag{24}$$

Here, $A^{(i)}$ is the scattering amplitude from the ith nanowire. It can be written as the sum of the contributions of the layers $A_n^{(i)}$, as it is done in Eq. (18), but at the moment we do not need this specification. When calculating the scattering intensity $|A_{\rm tot}|^2$, we separate the diagonal and the off-diagonal terms:

$$|A_{\rm tot}|^2 = \sum_{i=1}^{N_c} \left|A^{(i)}\right|^2 + \sum_{\substack{i,j=1 \\ i\neq j}}^{N_c} A^{(i)} A^{(j)*}, \tag{25}$$

the asterisk denotes the complex conjugate.

The scattering intensity (25) has to be averaged over a large number of coherence volumes. The nanowires in different coherence volumes have different and uncorrelated lengths and layer thicknesses. The average scattering amplitudes are equal for all nanowires, $\langle A\rangle = \langle A^{(i)}\rangle$, and do not depend on the nanowire number i. The scattering intensities are also equal, $\langle |A|^2\rangle = \langle |A^{(i)}|^2\rangle$. Since the structure parameters of the nanowires are not correlated, for $i \neq j$ one has $\langle A^{(i)} A^{(j)*}\rangle = \langle A^{(i)}\rangle \langle A^{(j)}\rangle^* = |\langle A\rangle|^2$. Then, the average intensity is

$$\langle |A_{\rm tot}|^2\rangle = N_c \langle |A|^2\rangle + N_c(N_c-1)|\langle A\rangle|^2. \tag{26}$$

The average intensity of a single nanowire $\langle |A|^2\rangle$ is given by Eq. (22). The average amplitude $\langle A\rangle$ is obtained from Eq. (16),

$$\langle A\rangle = \sum_{n=1}^{N} \frac{f_n}{iq_n}\left(e^{\Phi_{1,n}} - e^{\Phi_{1,n-1}}\right). \tag{27}$$

Figure 4 compares diffraction profiles calculated by Eq. (26) when the number of nanowires N_c within the coherence

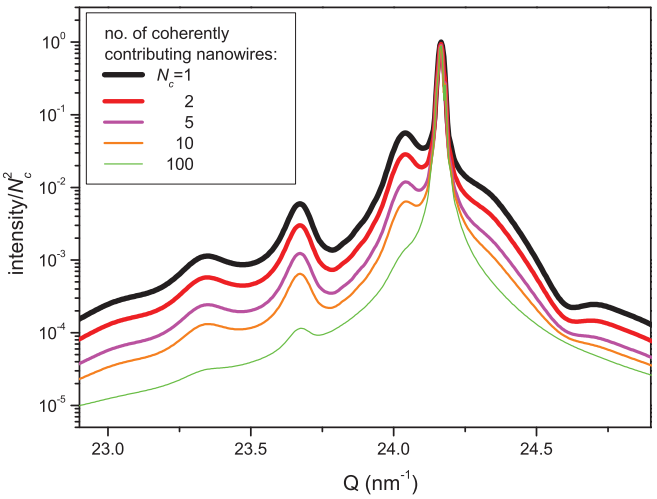

FIG. 4. (Color online) Variation of the diffraction profile with the number of nanowires that coherently add to diffraction.

volume is increased. The intensity is normalized by N_c^2 to keep all plots on the same scale. The top curve reproduces the calculation for sample 2 in Fig. 2. Further curves are calculated keeping the same parameters of the nanowires and varying only N_c. One can see from the plots that the interference between just two nanowires decreases the superstructure peaks by a factor of two. The satellite peaks remain visible, however, as long as the number of coherently contributing nanowires is less than 100.

IX. CONCLUSIONS

Typical ensembles of nanowires with axial heterostructures exhibit large fluctuations in nanowire heights and thicknesses of the individual layers in the heterostructure. Often they also possess a broad distribution of orientations. Nevertheless, the analysis of such superlattices can be performed similarly to the analysis of the familiar planar heterostructures by comparing measured and calculated x-ray diffraction patterns. For the example of self-induced GaN nanowires containing $In_xGa_{1-x}N$ quantum wells, we have demonstrated the successful determination of the superlattice period, thickness of the In-containing well layers, and In content in them. We have found that fluctuating strain (microstrain) broadens the GaN base peak. The superlattice peaks are notably broader due to layer thickness fluctuations, and the microstrain effects on them can be neglected. As a result of the broad orientational distribution in the samples that we have investigated, only one nanowire within the x-ray coherence volume contributes to diffraction. We show that, when the nanowire alignment is improved or the coherence is increased, the interference extinction results in decreasing intensity of the satellite reflections. The diffraction peaks persist, albeit damped, up to a hundred coherently illuminated nanowires.

ACKNOWLEDGMENTS

The authors thank Frank Grosse and Ivan Vartaniants for helpful discussions. The work has partly been funded by the German government BMBF project MONALISA and Deutsche Forschungsgemeinschaft (DFG) grant KA 3262/2-1.

[1] R. Agarwal, Small **4**, 1872 (2008).
[2] M. T. Björk, B. J. Ohlsson, T. Sass, A. I. Persson, C. Thelander, M. H. Magnusson, K. Deppert, L. R. Wallenberg, and L. Samuelson, Appl. Phys. Lett. **80**, 1058 (2002).
[3] J. Eymery, F. Rieutord, V. Favre-Nicolin, O. Robach, Y.-M. Niquet, L. Fröberg, T. Mårtensson, and L. Samuelson, Nano Lett. **7**, 2596 (2007).
[4] Y. Wu, R. Fan, and P. Yang, Nano Lett. **2**, 83 (2002).
[5] M. Hanke, C. Eisenschmidt, P. Werner, N. D. Zakharov, F. Syrowatka, F. Heyroth, P. Schäfer, and O. Konovalov, Phys. Rev. B **75**, 161303 (2007).
[6] M. S. Gudiksen, L. J. Lauhon, J. Wang, D. C. Smith, and C. M. Lieber, Nature (London) **415**, 617 (2002).
[7] J. Ristić, E. Calleja, M. A. Sánchez-García, J. M. Ulloa, J. Sánchez-Páramo, J. M. Calleja, U. Jahn, A. Trampert, and K. H. Ploog, Phys. Rev. B **68**, 125305 (2003).
[8] O. Landré, D. Camacho, C. Bougerol, Y. M. Niquet, V. Favre-Nicolin, G. Renaud, H. Renevier, and B. Daudin, Phys. Rev. B **81**, 153306 (2010).
[9] E. P. A. M. Bakkers, J. A. van Dam, S. de Franceschi, L. P. Kouwenhoven, M. Kaiser, M. Verheijen, H. Wondergem, and P. van der Sluis, Nat. Mater. **3**, 769 (2004).
[10] B. Mandl, J. Stangl, T. Mårtensson, A. Mikkelsen, J. Eriksson, L. Karlsson, G. Bauer, L. Samuelson, and W. Seifert, Nano Lett. **6**, 1817 (2006).
[11] L. Largeau, D. L. Dheeraj, M. Tchernycheva, G. E. Cirlin, and J. C. Harmand, Nanotechnology **19**, 155704 (2008).
[12] T. Kawamura, S. Bhunia, Y. Watanabe, S. Fujikawa, J. Matsui, Y. Kagoshima, and Y. Tsusaka, J. Appl. Phys. **97**, 084318 (2005).
[13] L. Horák, V. Holý, C. R. Staddon, N. R. S. Farley, S. V. Novikov, R. P. Campion, and C. T. Foxon, J. Appl. Phys. **104**, 103504 (2008).
[14] L. Geelhaar *et al.*, IEEE J. Sel. Top. Quantum Electron., doi:10.1109/JSTQE.2010.2098396.
[15] C. P. T. Svensson, W. Seifert, M. W. Larsson, L. R. Wallenberg, J. Stangl, G. Bauser, and L. Samuelson, Nanotechnology **16**, 936 (2005).
[16] I. A. Goldthorpe, A. F. Marshall, and P. C. McIntyre, Nano Lett. **8**, 4081 (2008).
[17] M. Keplinger, T. Mårtensson, J. Stangl, E. Wintersberger, B. Mandl, D. Kriegner, V. Holý, G. Bauer, K. Deppert, and L. Samuelson, Nano Lett. **9**, 1877 (2009).
[18] S. O. Mariager, C. B. Sørensen, M. Aagesen, J. Nygård, R. Feidenhans'l, and P. R. Willmott, Appl. Phys. Lett. **91**, 083106 (2007).
[19] V. Chamard, J. Stangl, S. Labat, B. Mandl, R. T. Lechner, and T. H. Metzger, J. Appl. Crystallogr. **41**, 272 (2008).
[20] L. Schubert, P. Werner, N. D. Zakharov, G. Gerth, F. M. Kolb, L. Long, U. Gösele, and T. Y. Tan, Appl. Phys. Lett. **84**, 4968 (2004).
[21] J. Johansson, C. P. T. Svensson, T. Mårtensson, L. Samuelson, and W. Seifert, J. Phys. Chem. B **109**, 13567 (2005).

[22]R. K. Debnath, R. Meijers, T. Richter, T. Stoica, R. Calarco, and H. Lüth, Appl. Phys. Lett. **90**, 123117 (2007).
[23]H. Sekiguchi, K. Kishino, and A. Kikuchi, Appl. Phys. Lett. **96**, 231104 (2010).
[24]L. E. Jensen, M. T. Björk, S. Jeppesen, A. I. Persson, B. J. Ohlsson, and L. Samuelson, Nano Lett. **4**, 1961 (2004).
[25]M. T. Borgström, G. Immink, B. Ketelaars, R. Algra, and E. P. A. M. Bakkers, Nat. Nanotechnology **2**, 541 (2007).
[26]T. Gotschke, T. Schumann, F. Limbach, T. Stoica, and R. Calarco, Appl. Phys. Lett. **98**, 103102 (2011).
[27]B. Kalache, P. R. Cabarrocas, and A. F. Morral, Jpn. J. Appl. Phys. **45**, L190 (2006).
[28]T. Clement, S. Ingole, S. Ketharanathan, J. Drucker, and S. T. Picrauxa, Appl. Phys. Lett. **89**, 163125 (2006).
[29]R. Calarco, R. J. Meijers, R. K. Debnath, T. Stoica, E. Sutter, and H. Lüth, Nano Lett. **7**, 2248 (2007).
[30]C. Chèze, L. Geelhaar, A. Trampert, and H. Riechert, Appl. Phys. Lett. **97**, 043101 (2010).
[31]C. Chèze, L. Geelhaar, A. Trampert, O. Brandt, and H. Riechert, Nano Lett. **10**, 3426 (2010).
[32]V. Consonni, M. Knelangen, L. Geelhaar, A. Trampert, and H. Riechert, Phys. Rev. B **81**, 085310 (2010).
[33]V. Consonni, M. Knelangen, U. Jahn, A. Trampert, L. Geelhaar, and H. Riechert, Appl. Phys. Lett. **95**, 241910 (2009).
[34]K. A. Dick, P. Caroff, J. Bolinsson, M. E. Messing, J. Johansson, K. Deppert, L. R. Wallenberg, and L. Samuelson, Semicond. Sci. Technol. **25**, 024009 (2010).
[35]V. M. Kaganer, B. Jenichen, and K. H. Ploog, J. Phys. D: Appl. Phys. **34**, 645 (2001).
[36]M. Hanke, M. Schmidbauer, and R. Köhler, J. Appl. Phys. **96**, 1959 (2004).
[37]B. E. Warren, *X-Ray Diffraction* (Addison-Wesley, Reading, Mass., 1969).
[38]M. Birkholz, *Thin Film Analysis by X-Ray Scattering* (Wiley, Weinheim, 2006).
[39]T. Adler and C. R. Houska, J. Appl. Phys. **50**, 3282 (1979).
[40]A. Leineweber and E. J. Mittemeijer, J. Appl. Cryst. **43**, 981 (2010).
[41]C. G. Darwin, Philos. Mag. Ser. 6 **43**, 800 (1922).
[42]D. Rafaja, V. Klemm, G. Schreiber, M. Knapp, and R. Kužel, J. Appl. Crystallogr. **37**, 613 (2004).
[43]D. Rafaja, V. Klemm, Ch. Wüstefeld, M. Motylenko, M. Dopita, M. Schwarz, T. Barsukova, and E. Kroke, Z. Kristallogr. Suppl. **27**, 15 (2008).